Materials Today Energy 21 (2021) 100753

Contents lists available at ScienceDirect

Materials Today Energy

journal homepage: www.journals.elsevier.com/materials-today-energy/

Highly efficient bismuth telluride–based thermoelectric microconverters

M. Maksymuk [a], T. Parashchuk [a, *], B. Dzundza [a], L. Nykyruy [a], L. Chernyak [b], Z. Dashevsky [c]

[a] Department of Physics and Chemistry of Solid Stated, Vasyl Stefanyk Precarpathian National University, Shevchenko 57, 76-000, Ivano-Frankivsk, Ukraine
[b] Department of Physics, University of Central Florida, Orlando, FL, 32816, USA
[c] Department of Materials Engineering, Ben-Gurion University, Beer-Sheva, 84-105, Israel

ARTICLE INFO

Article history:
Received 31 January 2021
Received in revised form
27 March 2021
Accepted 7 April 2021
Available online 15 April 2021

Keywords:
Microgenerators
Thermoelectric films
Flexible substrate
Efficiency of energy conversion
Flash evaporation

ABSTRACT

The flash evaporation method was used to fabricate high-performance *p*- and *n*-type Bi_2Te_3-based thermoelectric (TE) thin films. Optimized technological conditions of film preparation, as well as subsequent annealing, give the possibility to achieve a significant improvement in the TE properties of the designed TE films, which are state-of-the-art compared with bulk materials. Furthermore, a brand-new sandwich-layered design of the flexible film thermoelectric microconverter (FTEM) is offered here through the use of perforation cuts between *p*- and *n*-legs and a flexible polyimide substrate. Such a unique design makes it possible to avoid a rise in electrical resistance due to an increase in the number of elements in the microconverter. The dimensionless effective figure of merit $ZT \approx 0.6$ (including losses due to parasite heat flux along with the substrate, radiation, and conversion) and TE efficiency $\eta_{max} \approx 3.4\%$ were achieved for the FTEM prototype at the temperature difference ΔT of 100 K ($T_c = 300$ K). Therefore, the use of flash evaporation technology offers the possibility to produce large-scale film TE devices with high efficiency. Moreover, the applicability of the developed FTEM is demonstrated for a thermal detector with a high output voltage, which is used to determine a weak heat flux up to ~10^{-7} W.

1. Introduction

A typical commercial thermoelectric (TE) module consists of paired *p*- and *n*-type TE legs between two ceramic plates. Nevertheless, the thermal stress caused by the different thermal expansion coefficients of TE materials and ceramic plates would lead to a serious junction reliability problem, which limits the dimension and number of TE legs in the module [1–3]. The advantages of a thin film TE microconverter (FTEM) are large-scale integration of TE legs and high density of output power [4,5].

Recently, energy harvesting has been proposed as a promising method of supplying electric power to autonomous sensor network devices and mobile electrical instruments owing to the possibility of obtaining electric power from unused environmental energy, such as heat, light, and vibration [6]. It was found that direct energy microconverters for energy harvesting are more useful than standard electrical batteries. Previously, such generation systems were not considered important in small devices owing to insufficient power generation. However, they have been realized by drastically reducing the power consumption of electronic components as a result of advances in the field of electric energy storage, miniaturization, and optimization [7–15]. Besides, they can generate power from low-temperature heat sources [16,17].

The efficiency of such a TE converter (generator) could be estimated using the following expression [18]:

$$\eta_{max} = \frac{\Delta T}{T_h} \frac{\sqrt{1 + (ZT)_{av}} - 1}{\sqrt{1 + (ZT)_{av}} + \frac{T_c}{T_h}} \quad (1)$$

Here, T_h and T_c are the temperatures of the hot and cold sides, respectively, ΔT is the temperature difference between the hot and cold sides ($\Delta T = T_h - T_c$), and $(ZT)_{av}$ is the average dimensionless TE figure of merit, which is expressed as follows [19]:

$$(ZT)_{av} = \frac{1}{T_h - T_c} \int_{T_c}^{T_h} ZT \cdot dT \quad (2)$$

* Corresponding author. The Lukasiewicz Research Network, Krakow Institute of Technology, Zakopianska 73, 30-418, Krakow, Poland.
E-mail address: taras.parashchuk@kit.lukasiewicz.gov.pl (T. Parashchuk).

https://doi.org/10.1016/j.mtener.2021.100753
2468-6069/

For each *p*- and *n*-type TE leg, the *ZT* parameter depends on the main TE leg characteristics:

$$ZT = \frac{S^2\sigma}{\kappa}T \quad (3)$$

where S is the Seebeck coefficient, σ and κ are the electrical and thermal conductivity, respectively, and T is the absolute temperature.

Many different attempts, i.e., effect of the organic components on the TE properties of film samples [20], as well as different types of materials, i.e., $CoSb_3$ and Cu_2Se, was investigated to advance film thermoelectricity [21,22]. However, obtaining TE films with a high TE figure of merit *Z* at the moderated temperature is still a challenge. The maximum TE efficiency over the temperature range of 300–600 K has materials based on Bi_2Te_3, which are used for the fabrication of low-temperature TE generators [23–27]. Recently, high-efficiency *p*-type $Bi_{2-x}Sb_xTe_3$-based films with a dimensionless TE figure of merit *ZT* close to bulk samples were reported [28]. Fig. 1a and b show the temperature dependences of the *ZT* parameter over the temperature range of 200–400 K for *p*-type $Bi_{2-x}Sb_xTe_3$ bulk and film materials with a similar chemical composition and *n*-type $Bi_2Te_{3-y}Se_y$ bulk materials [26–29]. Unfortunately, so far, the situation with high-efficiency *n*-type Bi_2Te_3-based TE films is far from satisfactory.

So far, many different methods have been used to fabricate films based on *p*-type Bi_2Te_3-Sb_2Te_3 and *n*-type Bi_2Te_3-Bi_2Se_3, such as coevaporation, molecular beam epitaxy, magnetron sputtering, and pulsed laser deposition [30–36]. In this work, the fabrication of films was carried out using the flash evaporation technology [28]. Flash evaporation is a prominent technique for deposition of thin films of multicomponent alloys whose constituents have different vapor pressures. The main advantage of flash evaporation is that maintenance of critical vapor pressures of the components and temperatures of the boats is not required, unlike multisource thermal evaporation [37]. This makes it possible to obtain high accuracy of chemical composition (~0.05 at.%) for the fabricated films from the presynthesized ingot. Such high accuracy is extremely important due to the requirement of stabilization of the Fermi level in the optimal position to reach the highest possible TE power factor (PF) [38]. Even the latest method of film deposition (i.e., molecular beam epitaxy) cannot provide such high accuracy of chemical composition [39], which leads to lower TE performance.

An ultrathin polyimide substrate with a thickness of ~10 μm was used to minimize the negative heat losses. In addition, polyimide films have two significant advantages over other well-established types of substrates, i.e., extremely low thermal conductivity (~0.3 W $m^{-1}K^{-1}$) and high flexibility properties [40].

As with large-scale TE modules, a large number of TE elements should also be provided in the microconverter to increase the TE power. However, for typical serial connections of TE unicouples, the electrical resistance increases drastically as the number of TE elements increases. Here, we propose a unique sandwich-layered design of the film TE module to avoid such an increase in electrical resistance. The designed *p*- and *n*-type TE films will be deposited on both sides of the insulation substrate, each *p*- and *n*-film TE leg will consist of two layers with a parallel electrical connection, and the serial connection of *p*- and *n*-legs will be provided by metallic films through perforation cuts. The proposed original design of the parallel-serial connection sharply increases the reliability of the FTEM, even if the number of TE unicouples is huge. In this work, we also show the practical application of the FTEM for the development of sensitive thermal detectors up to 10^{-7} W.

2. Experimental procedure

2.1. Preparation of the TE thin film based on n- and p-type Bi_2Te_3 materials

Synthesis of $Bi_{2-x}Sb_xTe_3$ and $Bi_2Te_{3-y}Se_y$ alloys was carried out by direct melting of the components for 10 h at 1073 K in sealed quartz ampoules evacuated to a residual pressure of 10^{-5} mbar. Each ampoule was then taken from the furnace and quenched into cold water. Only high-purity (99.999) initial components were used for the synthesis. Before film fabrication, the obtained ingots were crushed into fine powders by ball milling in an argon atmosphere to prevent oxidation.

The *p*-type $Bi_{2-x}Sb_xTe_3$ and *n*-type $Bi_2Te_{3-y}Se_y$ alloy thin films were deposited via flash evaporation technology [28]. The temperature of the substrate for film preparation was $T_s = 523$ K; the evaporation velocity was $v_e = 0.1$ μm/min. After the evaporation process, all films were annealed in the same evaporation chamber at $T_t = 623$ K for 0.5 h in an atmosphere of pure argon at pressure $p = 9.1 \times 10^4$ Pa.

The structural analysis of the films was studied using an STOE STADI P X-ray diffractometer (by STOE & Cie GmbH, Germany) as per the modified Guinier geometry scheme using the transmission mode ($CuK\alpha_1$ radiation, concave Ge monochromator (111) of the Johann type; $2\theta/\omega$ scan, angle interval $10.000° \le 2\theta \le 125.185°$ with a scanning step of 0.015°; the scan time in step 100–230 s). The initial processing of experimental diffraction arrays was performed

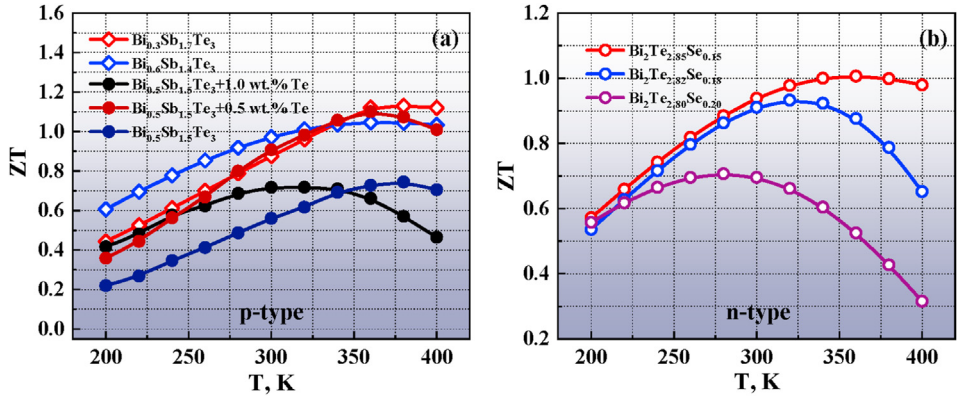

Fig. 1. The dimensionless figure of merit *ZT* as a function of temperature for (a) *p*-type bulk (open symbols) and film (close symbols) and (b) *n*-type bulk Bi_2Te_3-based thermoelectric materials over the temperature range of 200–400 K [26–29].

using the PowderCell (version 2.4) software packages. Scanning electron microscopy (SEM) images were taken using a Quanta 200 environmental scanning electron microscope equipped with energy-dispersive X-ray spectroscopy (EDS).

2.2. Measurement of TE properties for thin films

Measurements of the Seebeck coefficient S and electrical conductivity σ for TE thin films over the temperature range of 300–600 K were carried out using the developed measurement setup. The scheme and principle of operation of this measurement device are described in the study by Dzundza et al [41]. The accuracy of the temperature measurement was 0.1–0.2 K. The measurement error of the Seebeck coefficient and electrical conductivity was 6%.

The heat transfer in p-type $Bi_{2-x}Sb_xTe_3$ and n-type $Bi_2Te_{3-y}Se_y$ films on a flexible substrate was studied by the method of dynamic lattices [41–43]. It is based on the effect of excitation of the sample by two mutually interfering laser beams. As a result, the samples are characterized by a dynamic diffraction lattice, and the kinetics of the diffraction signal could be analyzed. Finally, the value of thermal diffusivity α was measured using this method. The measurement error of the thermal diffusivity was not more than 10%. The schematic view of the device with a description of the measurement approach is shown in the study by Dzundza et al [41]. The total thermal conductivity was calculated as per the following equation:

$$\kappa = \alpha \rho c_p \tag{4}$$

where ρ is the TE film density and c_p is the specific heat capacity calculated within the Dulong-Petit limit.

2.3. Measurement of output characteristics for the film TE unicouple

Measurements of the output characteristics (sensitivity and rise time) of a thermal detector based on the FTEM were carried out using the developed measurement setup, a schematic view of which is shown in Fig. 2. The source of radiation was a Q-switched CO_2 laser, with a pulse duration of 10^{-3} s and maximum intensity P of ~0.1 MW/cm^2 [44]. The beam was focused using a ZnSe lens. The rise time from the thermal detector was measured using a Tektronix preamplifier ADA400A and displayed on a Tektronix e-Scope TDS 3054B. The laser pulse duration was measured using a Ge:Au detector. The measurement error of sensitivity (the ratio of the output voltage to output heat flux) and rise time was 3%.

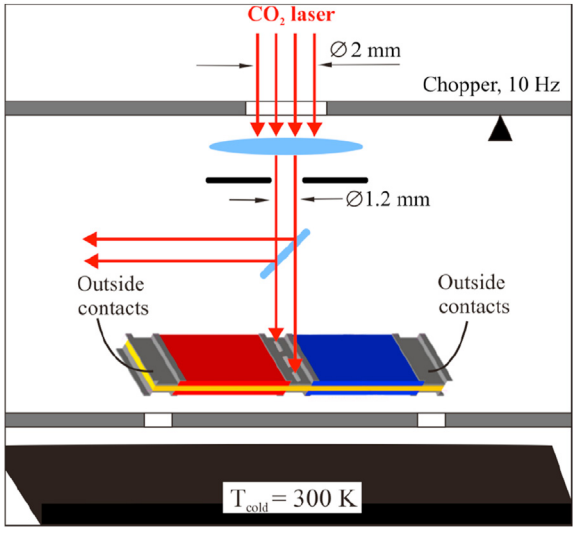

Fig. 2. Schematic view of the experimental setup for measuring the output characteristics (sensitivity and rise time) of the film thermoelectric unicouple.

3. Result and discussion

3.1. Crystal structure and microstructural analyses

Bi_2Te_3-based alloys crystallize with a layered crystal structure. The five-layered structure with mixed covalent-ionic interaction consists of two Bi layers sandwiched between three Te layers connected by weak van der Waals forces. This layered structure is a good precursor of low lattice thermal conductivity, and anisotropy of transport properties is typically observed for these compounds.

Because strong texturization of the sample morphology is expected for Bi_2Te_3 alloys, we carried out an X-ray diffraction (XRD) analysis of the specimens after synthesis and the films after annealing. The structural and microstructural properties of p-type $Bi_{2-x}Sb_xTe_3$ films were studied in detail in our recent work [28]; therefore, here, we focus on the structural and microstructural analyses of n-type $Bi_2Te_{3-y}Se_y$ films. The refined experimental patterns for the representative $Bi_2Te_{2.4}Se_{0.6}$ specimen after synthesis are depicted in Fig. 3a. The observed diffraction reflections of the as-cast sample were indexed in the rhombohedral structure (COD #9012064). Any impurity phases were not detected within the measurement limit of the instrument. The SEM analysis confirms the single-phase nature and absence of impurity phases in the investigated $Bi_{2-x}Sb_xTe_3$ ingot sample (Fig. 3b). The estimated chemical composition for this sample is similar to the nominal composition.

Fig. 3c demonstrates experimental XRD patterns of the n-type $Bi_2Te_{3-y}Se_y$ films on a flexible polyimide substrate. The reflections are very similar to those received in the study by Parashchuk et al [28] for the $Bi_{2-x}Sb_xTe_3$ films. Both n-type $Bi_{2-x}Sb_xTe_3$ and p-type $Bi_2Te_{3-y}Se_3$ films show high intensity of (006) and (0015) peaks, indicating high texturization in [00l] crystal direction. The secondary emission image of the $Bi_2Te_{3-y}Se_y$ film confirms a nice deposition of the material on the polyimide substrate and formation of plate-shaped grains, which is typical for Bi_2Te_3-based alloys (Fig. 3d). The average grain sizes for the investigated films are in the range of 1–3 μm. Not a single pore was observed on the surface of the investigated film, proving that the flash evaporation technology is a good method for preparing films with high quality.

3.2. Transport properties

The thickness of the substrate and the film is an important parameter that affected heat transport through the film. As per Fourier's law, the ratio of heat flow Q_f/Q_s through the film and substrate is related to the thermal conductivity and the thickness of the film and the substrate as per the following expression:

$$\frac{Q_f}{Q_s} \sim \frac{\kappa_f d_f}{\kappa_s d_s} \tag{5}$$

Here, d_f and d_s are the thicknesses of the film and the substrate and κ_f and κ_s are the thermal conductivities of the film and the substrate, respectively. As the thermal conductivity of the film must be low κ_f, the optimal TE performance of the film requires the lowest possible values of thermal conductivity κ_s and thickness d_s for the substrate and the highest value of thickness d_f for the film to have high carrier mobility.

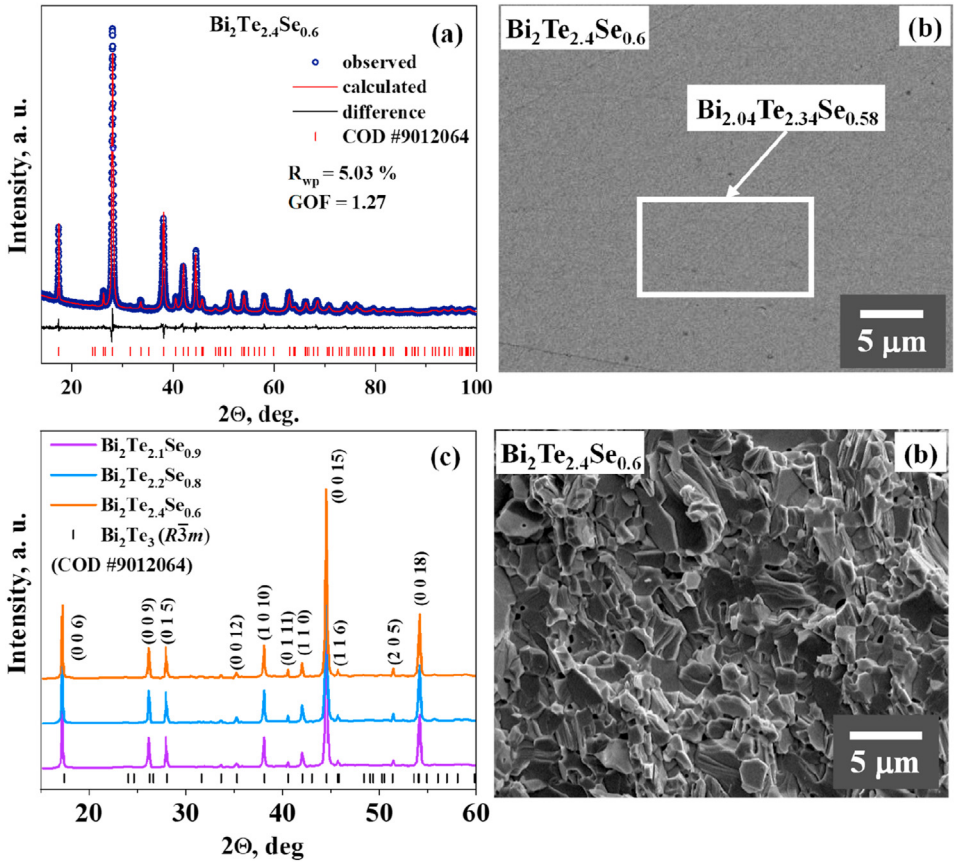

Fig. 3. (a) Refined powder XRD pattern of the $Bi_2Te_{2.4}Se_{0.6}$ sample after synthesis. (b) SEM image and EDS analysis of the polished surface for the $Bi_2Te_{2.4}Se_{0.6}$ sample after synthesis. (c) Experimental XRD patterns of $Bi_2Te_{3-y}Se_y$ films on a polyimide substrate. (d) Secondary emission image for the $Bi_2Te_{2.4}Se_{0.6}$ thin film on a polyimide substrate. SEM = scanning electron microscopy, EDS = energy-dispersive X-ray spectroscopy.

A detailed investigation of the thickness effect on the mechanical stability and TE properties of Bi_2Te_3-based thin films was carried out in the study by Goltzman et al [45]. Film thickness larger than ~5 μm creates microcracks in the film after film deposition and thermal annealing owing to different linear expansion coefficients between the deposited TE film and the polyimide substrate. Therefore, all the investigated films were prepared with an optimal thickness of ~5 μm on an ultrathin substrate with a thickness of ~10 μm. Such film and substrate thicknesses also provide sufficient flexibility to the device.

Fig. 4a represents the Seebeck coefficient S for $Bi_{2-x}Sb_xTe_3$ (x = 1.5, 1.55, 1.6) films over the entire temperature range of 300–600 K. The Seebeck coefficient for these series of films shows positive values in the given temperature range, indicating p-type conductivity. The value of the Seebeck coefficient at 300 K decreases from ~190 μV/K to ~170 μV/K with an increase in the nominal Sb concentration in $Bi_{2-x}Sb_xTe_3$ films from x = 1.5 to x = 1.6, which is in line with previously reported data for the bulk samples [29]. The temperature trends of the Seebeck coefficient show a maximum value and then go down owing to the effect of intrinsic carriers, which is typical for narrow-band semiconductors.

The electrical conductivity of the investigated films decreases over the investigated temperature range, indicating a metallic tendency (Fig. 4b). The excellent TE performance of the fabricated films was confirmed by the estimation of the PF $S^2\sigma$ (Fig. 4c). The maximum value of $S^2\sigma$ is ≈50 μWcm^{-1}K^{-2}, which is practically equal to the PF for the best bulk samples with the same chemical composition [29].

The TE properties of $Bi_2Te_{3-y}Se_y$ films were studied to design the best n-type leg in terms of energy conversion for the construction of the FTEM. The Seebeck coefficient is negative for all films, indicating electrons as the major carrier. The absolute values of the Seebeck coefficient for n-$Bi_2Te_{3-y}Se_y$ film samples decrease from ~220 μV/K to ~175 μV/K at T = 300 K with the Se content increasing from y = 0.1 to y = 0.6, indicating an increase in the carrier concentration (Fig. 4d). Such a behavior of the Seebeck coefficient in the Bi_2Te_3–Bi_2Se_3 solid solutions is close to the $Bi_2Te_{3-y}Se_y$ bulk compounds with a similar chemical composition [46–49]. The temperature trends of the S value first increase, reach the maximum value, and then decrease owing to the intrinsic conduction regime, which is very common for narrow-bandgap semiconductors. As the Se content in $Bi_2Te_{3-y}Se_y$ films increases, the maximum of the Seebeck coefficient shifts toward higher temperatures owing to the increase in concentration.

The electrical conductivity σ decreases with increasing temperature over the investigated temperature range, indicating metallic behavior, as shown in Fig. 4e. The value of σ demonstrates an opposite trend to the Seebeck coefficient and increases with the increase in the Se content, which is well explained by the inverse dependences of S and σ on carrier concentration n. We do not observe any atypical decrease in the electrical conductivity in our films compared with bulk $Bi_2Te_{3-y}Se_y$ samples of the same composition, indicating that the mobility of the films is similar in the films and bulk samples.

Fig. 4f shows the PF $S^2\sigma$ as a function of temperature for $Bi_2Te_{3-y}Se_y$ films. The maximum value of the PF ~41 μW cm^{-1}K^{-2} was

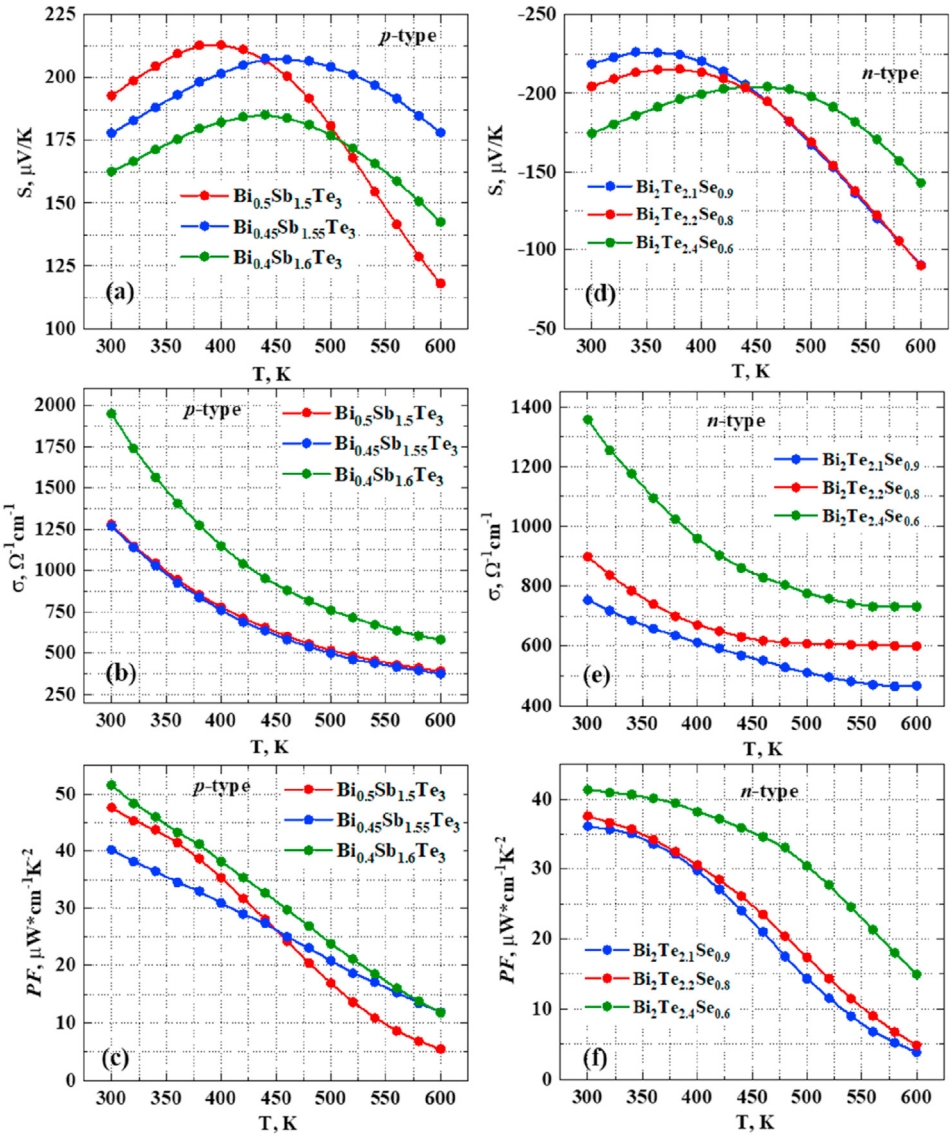

Fig. 4. Seebeck coefficient S (a and d), electrical conductivity σ (b and e), and power factor $S^2\sigma$ (c and f) as a function of temperature for p-type $Bi_{2-x}Sb_xTe_3$ (a–c) and n-type $Bi_2Te_{3-y}Se_y$ (d–f) thermoelectric films, respectively.

obtained for the $Bi_2Te_{3-y}Se_y$ $y = 0.6$ film at 300 K owing to the optimized position of the chemical potential. Such values of the PF agree well with the PF reported for the bulk samples, with close chemical composition indicating the excellent TE performance of the investigated films. Furthermore, the value of the PF obtained in this work is among the highest values reported for n-type $Bi_2Te_{3-y}Se_y$-based films at any time, opening their potential for the FTEM fabrication.

Table 1 shows the measured TE properties (Seebeck coefficient S, electrical conductivity σ, and thermal conductivity κ) for p-$Bi_{0.4}Sb_{1.6}Te_3$ and n-$Bi_2Te_{2.4}Se_{0.6}$ films at $T = 300$ K. It should be mentioned that the thermal conductivity κ was measured via the dynamic lattice method in the direction along with the film. Consequently, the measurement of all three parameters (Seebeck coefficient S, electrical conductivity σ, and thermal conductivity κ) was carried out in the same crystallographic direction along with the film. Only this method is accurate for estimating the TE figure of merit Z for anisotropic Bi_2Te_3-based alloys.

The value of the total thermal conductivity as a function of temperature was calculated by summing up the lattice κ_L and the electronic κ_e thermal conductivity ($\kappa = \kappa_L + \kappa_e$). The lattice thermal conductivity at $T = 300$ K was estimated from the direct measurement of the thermal diffusivity and is shown in Table 1. The lattice thermal conductivity as a function of temperature was assumed to be similar to the bulk material [29]. The values of κ_e have been obtained using the Wiedemann-Franz law:

Table 1
Thermoelectric properties of p- and n-type $(Bi,Sb)_2(Te,Se)_3$-based films at $T = 300$ K.

Material	Seebeck coefficient (S; μVK^{-1})	Electrical conductivity (σ; Ω^{-1}cm^{-1})	Thermal conductivity (κ; Wm^{-1}K^{-1})	Figure of merit ($Z \times 10^3$, K^{-1})
p-$Bi_{0.5}Sb_{1.5}Te_3$	190	1270	1.5	3.1
n-$Bi_2Te_{2.1}Se_{0.9}$	−220	750	1.3	2.8

$$\kappa_e = L_0 \sigma T \tag{6}$$

where L is the Lorentz number, which can be calculated using the following equation:

$$L = \left(\frac{k_0}{e}\right)^2 \left[3\frac{F_2(\mu^*)}{F_0(\mu^*)} - \left(2\frac{F_2(\mu^*)}{F_0(\mu^*)}\right)^2\right] \tag{7}$$

where k_0 is the Boltzmann constant, e is the electron charge, and $F(\mu^*)$ is Fermi-Dirac integrals. The parameter $\mu^* = (E_F - E_V)/k_0T$ for p-type material ($\mu^* = (E_C - E_F)/k_0T$, for n-type material) is the reduced Fermi energy, where E_C and E_V are the conduction band minimum and valence band maximum, respectively. E_F is the Fermi energy, and T is the absolute temperature.

At the acoustic phonon scattering of charge carriers, the reduced Fermi energy μ^* can be obtained by fitting the Seebeck coefficient using Eq. (8):

$$S = \frac{k_0}{e}\left[\frac{(r+2)F_{r+1}(\mu^*)}{(r+1)F_r(\mu^*)} - \mu^*\right] \tag{8}$$

Fig. 5a and b shows the estimated total thermal conductivity as a function of temperature for the investigated n- and p-type Bi_2Te_3-based films. All temperature trends of κ decrease over the investigated temperature range, indicating metallic conduction.

Combining the measured Seebeck coefficient S, electrical conductivity σ, and estimated thermal conductivity κ, we calculated the TE figure of merit Z for n- and p-type conductivity Bi_2Te_3-based films (Fig. 5c and d). Thanks to the high efficiency of the flash evaporation technology and sufficiently large thickness of the films, a high value of Z parameter around ~3.0 × 10^{-3} was obtained for the best n-$Bi_2(Te,Se)_3$ and p-$(Bi,Sb)Te_3$ films over the temperature range of 300–400 K. The values of the TE figure of merit achieved in this work are among the highest values at any time reported for film samples.

3.3. Fabrication technology of the proposed FTEM

Here, we report on the developed technological process for the fabrication of an FTEM. The main goal of such an FTEM is to show high TE performance with a ZT up to 1.0, as is already obtained for bulk TE generators based on Bi_2Te_3 alloys. The best in terms of energy conversion Bi_2Te_3-based films obtained in this work were used in the fabrication of the FTEM. We used the $Bi_{0.5}Sb_{1.5}Te_3$ alloy with a TE figure of merit (Z) of 3.1 at $T = 300$ K as a p-type leg of the film unicouple, and the $Bi_2Te_{2.9}Se_{0.1}$ alloy with a Z of 2.8 at $T = 300$ K was found to be the best n-type film. Consequently, the TE performance of the investigated films is as high as for the bulk materials, which is one of the main requirements for the FTEM with high efficiency.

However, a large number of TE unicouples are needed for construction of the FTEM with high electric power output. In this case, except for high TE performance for n- and p-type films of the FTEM, a minimal contact resistance should be provided for the device. Owing to the large number of TE unicouples connected in serial connection, a drastic increase in electrical resistance (decrease of TE performance) is observed in typical FTEMs. To avoid this problem, we propose a unique design of the film TE generator with high TE efficiency. The technological procedure for fabrication of such an FTEM is described as follows:

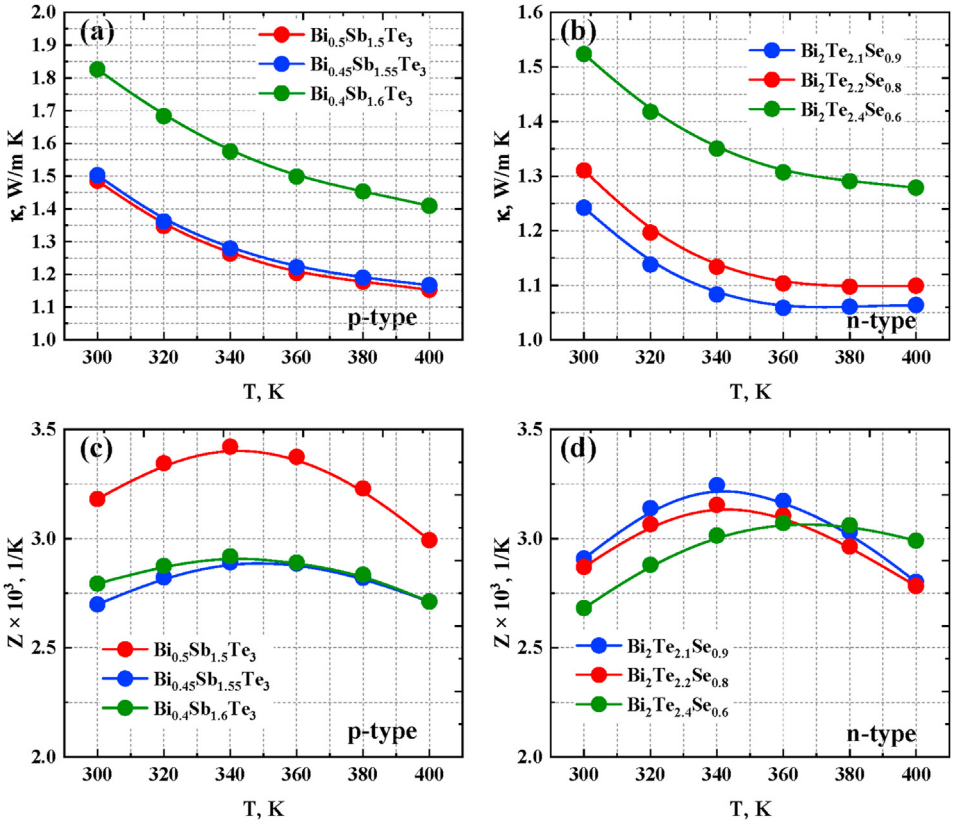

Fig. 5. Thermal conductivity κ (a and b) and thermoelectric figure of merit Z (c and d) as a function of temperature for p-type $Bi_{2-x}Sb_xTe_3$ (a and c) and n-type $Bi_2Te_{3-y}Se_y$ (b and d) thermoelectric films, respectively.

1. Deposition of *p*-type $Bi_{0.5}Sb_{1.5}Te_3$ films with a thickness of ~5 μm on both sides of the polyimide substrate with a thickness of ~10 μm using flash evaporation
2. Deposition of *n*-type $Bi_2Te_{2.9}Se_{0.1}$ films with a thickness of ~5 μm on both sides of the polyimide substrate using flash evaporation
3. Fabrication of perforations between *p*- and *n*-type films, which will provide the required electrical connection. The length of the cut is ~0.25 mm, and the distance between the cuts is ~1 mm; such cuts can be made using a GaAs laser.
4. Fabrication of the electrical connection (metallic layers of Cr with a thickness of ~0.1 μm and Au with a thickness of ~0.1 μm) between *p*- and *n*-type films on both sides of the polyimide substrate and inside the perforation cuts by an evaporating metallic layer. Such a multilayer electrode structure ensures thermal stability and provides a good electrical connection for the device [50].

A schematic view of the main stages of fabrication of the flexible FTEM based on *p*-type $Bi_{0.5}Sb_{1.5}Te_3$ and *n*-type $Bi_2Te_{2.9}Se_{0.1}$ TE materials is shown in Fig. 6.

As a result, the developed flexible FTEM consists of *p*- and *n*-type TE films on both sides of the substrate with parallel electric connections of each type of film (Fig. 6(1–2)). Additional serial connections of *p*- and *n*-legs were provided using Au and Cr metallic layers placed between the legs and internal perforation cuts in the polyimide substrate (Fig. 6(3–4)). As the films are evaporated on both sides of the substrate, the required number of serially connected legs is much lower. Furthermore, such a serial-parallel connection sharply increased the reliability of the FTEM, even if it consists of a large number of TE unicouples. Electrical reliability *N* of the FTEM depends on the number of thermoelements *n* and the type of electrical connection between *p*- and *n*-legs. The use of typical serial connections of TE film unicouples for the FTEM fabrication shows significantly lower reliability of the device with the increase in the number of film unicouples *n* [45]. On the contrary, the reliability of the FTEM with the proposed serial-parallel connection does not decrease, even if the number of TE unicouples is higher than $N \geq 100$ (Fig. 7). Furthermore, thanks to the proposed design, two films of each type (*n* and *p*) connected in parallel are responsible for electrical connection. Therefore, if one film is destroyed, the electrical circle in the FTEM will continue to work over the second film. As far as we know, such a solution has never been proposed before and can be a breakthrough mechanism for advancing TE film technologies.

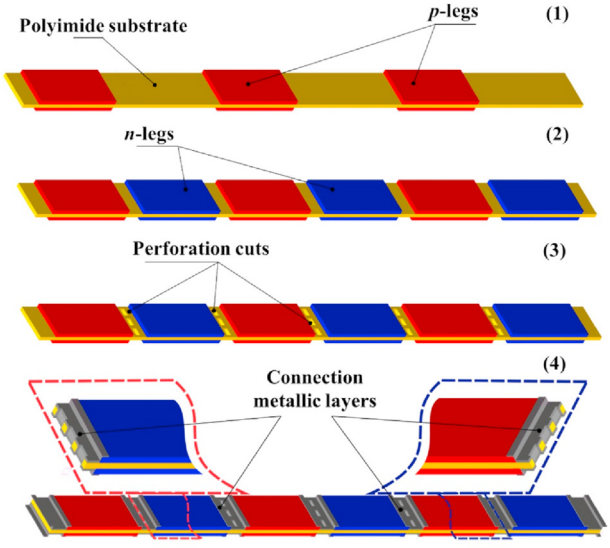

Fig. 6. Schematic view of the main stages for the fabrication of the flexible FTEM. FTEM = film thermoelectric microconverter.

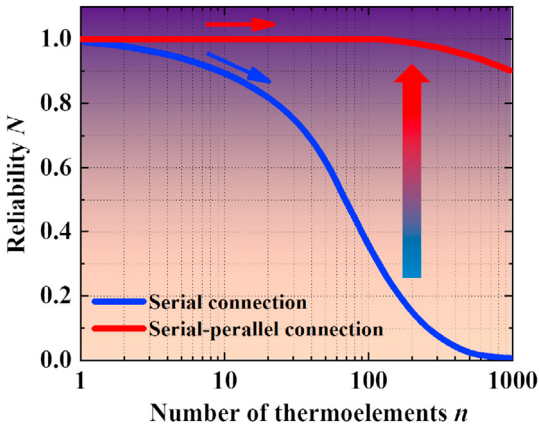

Fig. 7. The estimated reliability *N* vs a number of thermoelectric unicouples *n* of the FTEM (the reliability of the individual element was assumed as 0.99) for a serial electrical connection of *p*- and *n*-legs [45] and proposed serial-parallel electrical connection of *p*- and *n*-legs. FTEM = film thermoelectric microconverter.

3.4. Calculations of the output characteristics of the FTEM

This section clarifies the method for estimating the energy parameters for the FTEM, which depends on the distributions of temperature $T(x,y,z)$ and heat flux density $\vec{q} = -\kappa\nabla T$ in the TE legs. The distributions were determined by solving the boundary task of the stationary thermal conduction for each film leg, which takes into account thermal losses due to radiation and convection from the surfaces of the film TE legs, as well as losses due to thermal conduction of the polyimide substrate. Such a three-dimensional heat flux task was solved by the numerical finite element method in the COMSOL Multiphysics software. The model of the TE leg used to solve the task is shown in Fig.8.

The boundary conditions of the heat conduction equation under review take into account that the plane of the heat-absorbing junction of the film leg is maintained at temperature T_h and the plane of the heat-generating junction is maintained at temperature T_c. These temperatures depend on the heat source and the heat reset system, are assumed to be constant, and are given before the calculation. On the film surface, the heat

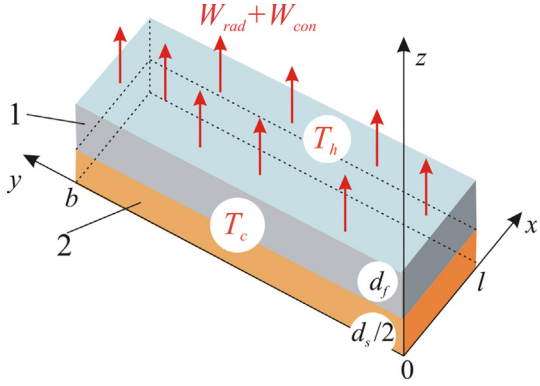

Fig. 8. Physical model of the film thermoelectric leg: (1) thermoelectric film; (2) substrate.

exchanging the environment proceeds owing to heat radiation W_{rad} and heat convection W_{conv}. The remaining faces are considered adiabatically isolated.

The input characteristics of the *n*- and *p*-type film materials, substrate geometric dimensions, and other physical values used in the calculation are given in Table 2. Examples of the temperature distribution of the *n*- and *p*-type film TE legs are shown in Fig. 9a and b.

The components of the vector of the heat flux density $\vec{q}$ over the leg are also the results of solving the heat flux task. These values were used to determine the portion of the heat transferred through the TE film for the total heat flux through the leg.

The heat balance over the leg can be written in the following form:

$$W = W_{f\ out} + W_{s\ out} + W_{rad} + W_{con} \tag{9}$$

where $W = W_{f\ in} + W_{s\ in}$ is the total amount of heat absorbed by the leg, $W_{f\ in}$ and $W_{f\ out}$ as well as $W_{s\ in}$ and $W_{s\ out}$ are the input and output heat through the film and substrate, respectively, and W_{rad} and W_{con} are heat losses due to radiation and convection, respectively.

The components of the heat balance equation were calculated using the following formulas:

Table 2
Input data for numerical simulation.

Parameter	Value
Temperature of the hot side, T_h	400 K
Temperature of the cold side, T_c	300 K
Ambient temperature, T_0	298 K
Thermal conductivity of the *p*-leg, κ_p ($T = 300$ K)	1.5 W m^{-1}K^{-1}
Thermal conductivity of the *n*-leg, κ_n ($T = 300$ K)	1.3 W m^{-1}K^{-1}
Thermal conductivity of the polyimide substrate, κ_s ($T = 300$ K)	0.3 W m^{-1}K^{-1}
Thickness of the film thermoelectric leg, d_f	2, 5, and 10 μm
Thickness of the polyimide substrate, d_s	10 μm
Length of the film thermoelectric leg, l	1, 2, 4 mm
Width of the leg, b	4 mm
Coefficient of the convective heat transfer, α	10 W m^{-2}K^{-1}
Emissivity of the thermoelectric layer, ε	0.8

$$W_{f\ in} = \int_{d_s/2}^{d_f}\int_{0}^{b}\left|-\kappa_f\frac{dT}{dx}\right|_{x=l} dzdy, \quad W_{f\ out} = \int_{d_s/2}^{d_f}\int_{0}^{b}\left|-\kappa_f\frac{dT}{dx}\right|_{x=0} dzdy,$$

$$W_{s\ in} = \int_{0}^{d_s/2}\int_{0}^{b}\left|-\kappa_s\frac{dT}{dx}\right|_{x=l} dzdy, \quad W_{s\ out} = \int_{0}^{d_s/2}\int_{0}^{b}\left|-\kappa_s\frac{dT}{dx}\right|_{x=0} dzdy,$$

$$W_{rad} + W_{\text{cov}} = \int_{0}^{l}\int_{0}^{b}\left|-\kappa_f\frac{dT}{dz}\right|_{z=d_f} dxdy. \tag{10}$$

The results of the calculations for the portion of the heat transferred through the film $\frac{W_{f\ out}W_{f\ out}}{W\ W}$ and through the substrate $\frac{W_{s\ out}}{W}$ and the portion of the heat loss due to radiation and convection $\frac{W_{rad}+W_{con}}{W}$ are shown in Table 3.

To calculate the efficiency of the FTEM, the heat transfer over the substrate and the heat transfer to the environment can be roughly taken into account when introducing the effective thermal conductivity of the *p*- and *n*-legs using the following equations:

$$\kappa_{ef}^{p} = \kappa_f^{p}\frac{W^{p}}{W_{f\ out}^{p}}, \quad \kappa_{ef}^{n} = \kappa_f^{n}\frac{W^{n}}{W_{f\ out}^{n}} \tag{11}$$

The effective figure of merit Z_{ef} of the film TE unicouple is then defined as follows:

$$Z_{ef} = \frac{(s_p - s_n)^2}{\left(\sqrt{\kappa_{ef}^{p}/\sigma_p} + \sqrt{\kappa_{ef}^{n}/\sigma_n}\right)^2} \tag{12}$$

And efficiency η_{max} FTEM is calculated using Eq. (1), in which $Z = Z_{ef}$.

The following mathematical expressions were used to estimate the open-circuit voltage V, resistance R of the FTEM, load current I_L in the circuit with load $R_L \approx R$, load voltage V_L, and generated power P_L:

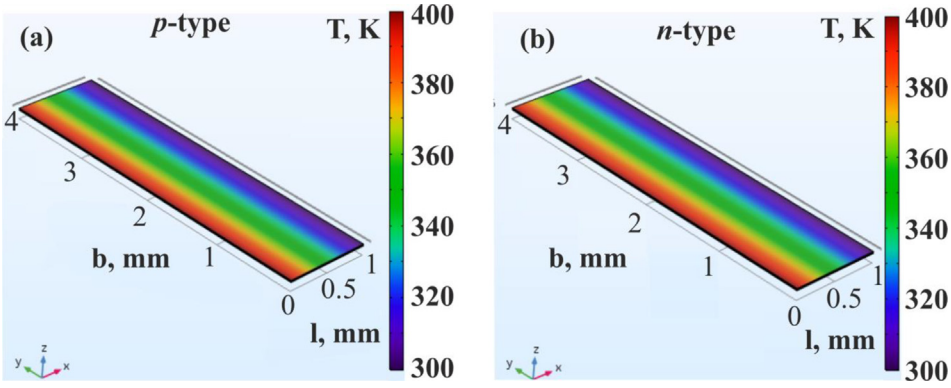

Fig. 9. Temperature profile on the film surface of the *p*-type (a) and *n*-type type (b) thermoelectric leg with the film thickness $d_f = 10$ μm.

Table 3
Heat components for the *p*-type film leg based on $Bi_{0.5}Sb_{1.5}Te_3$ and for the *n*-type film leg based on $Bi_2Te_{2.9}Se_{0.1}$.

d_f, μm	*l*, mm	*p*-type			*n*-type		
		$W_{f\ out}/W$	$W_{s\ out}/W$	$(W_{rad}+W_{con})/W$	$W_{f\ out}/W$	$W_{s\ out}/W$	$(W_{rad}+W_{con})/W$
2	1	0.15	0.12	0.73	0.13	0.14	0.73
2	2	0.05	0.04	0.91	0.04	0.05	0.91
2	4	0.01	0.01	0.98	0.01	0.01	0.98
5	1	0.30	0.10	0.6	025	0.12	0.63
5	2	0.10	0.04	0.86	0.10	0.05	0.85
5	4	0.03	0.01	0.96	0.03	0.01	0.96
10	1	0.64	0.05	0.31	0.53	0.06	0.41
10	2	0.34	0.03	0.63	0.28	0.04	0.68
10	4	0.08	0.01	0.91	0.07	0.01	0.92

$$\begin{aligned} V &= N(s_p - s_n)(T_h - T_c), \\ R &= (1/\sigma_p + 1/\sigma_n)\frac{l}{2d_f b}, \\ I_L &= V/(R_L + R), \\ V_L &= I_L R_L, \\ P_L &= I_L V_L, \end{aligned} \tag{13}$$

where s_n, s_p, σ_n, and σ_p are the experimental values of the corresponding film material properties shown in Table 1.

The calculated output characteristics of the FTEM with the number of thermocouples $N = 100$ are shown in Table 4.

These promising results demonstrate the high performance of FTEMs and open up the possibility of the practical application of such modules.

4. Development of a thermal detector

Thermal TE detectors are used to measure the heat flux [51]. The principle of their operation is described as follows: the input heat creates a temperature gradient across the sensor, and owing to the TE effect, this temperature gradient generates electricity. A schematic view of the proposed thermal detector is presented in Fig. 10. The electric voltage was excited by heating the hot side of the film TE unicouples with a chopper modulated aperture with a frequency of 1 kHz. The cold side temperature of the film TE unicouples is stabilized by a black body at the temperature of 300 K.

Table 4
Output characteristics of the FTEM at $T_h = 400$ K and $T_c = 300$ K (number of thermocouples $N = 100$, total film thickness $d_f = 10$ μm, leg length $l = 1$ mm, leg width $b = 4$ mm).

$(Z_{ef}T)_{av}$	η_{max}, %	*R*, Ω	I_L, mA	V_L, V	P_L, mW
0.6	3.4	70	30	3	90

FTEM = film thermoelectric microconverter.

The sensitivity $S_{v\text{-}w}$ of the thermal detector can be found as follows:

$$S_{V-W} = \frac{V}{W} \tag{14}$$

where *V* is the output voltage and *W* is the input heat flux.

$$V = (S_p - S_n)n\Delta T \tag{15}$$

Here, S_n and S_p are the Seebeck coefficient for *n*- and *p*-type films, respectively, *n* is the number of TE unicouples, and ΔT is the temperature gradient.

The input heat flux can be found as follows: :

$$W = n(\kappa_n + \kappa_p)\frac{bd}{l}\Delta T \tag{16}$$

For a film TE micromodule with dimensions $l = 1$ mm, $b = 2$ mm, and $d = 10$ μm and assuming similar values for S_n and S_p and κ_n and κ_p, the sensitivity $S_{v\text{-}w}$ for the thermal detector is as follows:

$$S_{V-W} = \frac{S_{av}}{\kappa_{ef}}\frac{l}{bd} \sim 10\frac{V}{W} \tag{17}$$

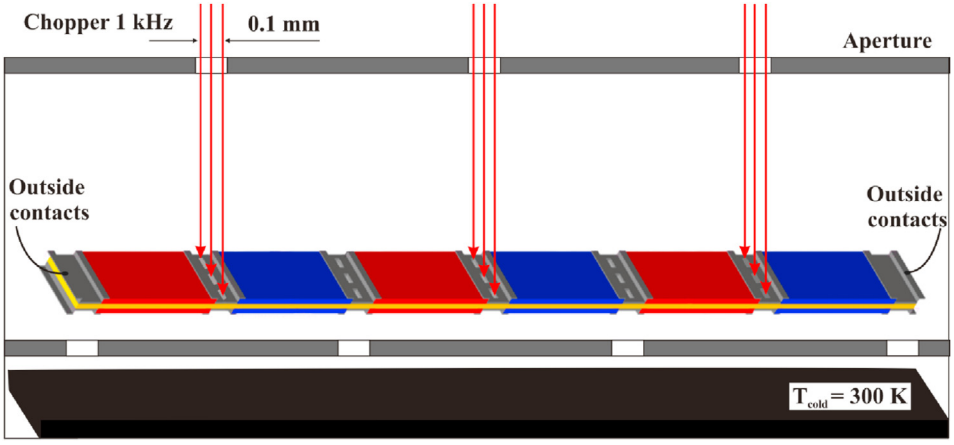

Fig. 10. Schematic view of the thermal detector based on the FTEM. FTEM = film thermoelectric microconverter.

The rise time of the FTEM-based thermal detector can be found as follows [52]:

$$\tau \approx \frac{c\rho l^2}{\kappa_{ef}} \quad (18)$$

where ρ is the TE film density and c is the specific heat capacity. For thermal sensor based on the FTEM with a height of n- and p-legs $l = 1$ mm, $\tau \approx 100$ ms. The measured values of sensitivity and rise time for the film TE unicouple are in good agreement with the calculated data.

5. Conclusions

The TE properties of p-type $B_{2-x}Sb_xTe_3$ and n-$Bi_2Te_{3-y}Se_y$ films were studied. Thanks to the optimized technological conditions with further annealing, the TE figure of merit Z for the investigated films reaches a high value $Z \approx 2.8 \times 10^{-3}$ K $^{-1}$ for n-type and 3.1×10^{-3} K^{-1} for p-type films at 300 K, which are comparable with the best bulk samples with similar composition.

Furthermore, here, we report on the development of a unique design of the flexible FTEM based on p-type $B_{2-x}Sb_xTe_3$ and n-$Bi_2Te_{3-y}Se_y$ film materials on a thin polyimide substrate. For the proposed FTEM (the leg size $l = 1$ mm), a dimensionless figure of merit $ZT \approx 0.6$ (taking into account all heat losses) and TE efficiency $\eta_{max} \approx 3.6\%$ at a temperature difference ΔT of 100 K ($T_c = 300$ K) was achieved, which is a state-of-the-art result even if compared with the best available microconverters.

The flexible FTEM consists of p- and n-type TE films with a thickness of ~5 μm on both sides of the substrate. The parallel electric connection of each type of film on both sides of the substrate and the serial connection of p- and n-legs by Au and Cr metallic films were enabled by perforation cuts in the polyimide substrate. This parallel-serial connection sharply increases the reliability of the FTEM, and if one n- and p-type film is destroyed, the electrical circle in the FTEM will continue to work over the second film. As far as we know, such a solution has never been discussed before and can be a breakthrough mechanism for advancing TE film technologies.

The simple technological method of flash evaporation for the FTEM fabrication and the possibility to build a device with much higher electrical power (by increasing the number of TE couples) indicate a high practical interest in the proposed FTEM for real-world applications.

As an example of a practical application, we show the FTEM-based thermal detector that was developed herein. The resulting sensitivity of the detector $S_{V\text{-}W} \approx 10$ V/W makes it very useful for detecting weak heat flux as low as ~10^{-7} W.

Credit author statement

M. Maksymuk: Visualization, Data Curation**,** Software**, T.Parashchuk:** Investigation, Methodology, Writing - Original draft preparation**, B. Dzundza:** Formal analysis, Visualization**, L. Nykyruy:** Conceptualization, Software, **L. Cherniak:** Formal analysis, Validation, **Z. Dashevsky:** Writing - Review & Editing, Methodology, Supervision.

Declaration of competing interest

The authors declare that they have no known competing financial interests or personal relationships that could have appeared to influence the work reported in this paper.

Acknowledgments

M.M. and T.P. contributed equally.

References

[1] G.S. Nolas, J. Sharp, H.J. Goldsmid, Thermoelectrics: Basic Principles and New Materials Developments, Springer-Verlag, Berlin, 2001.
[2]] D.M. Rowe, Thermoelectrics Handbook: Macro to Nano, CRC Press, Taylor and Francis Group, London, New York, Boca Raton, 2006.
[3] T. Parashchuka, N. Sidorenko, L. Ivantsov, A. Sorokin, M. Maksymuk, B. Dzundza, Z. Dashevsky, Development of a solid-state multi-stage thermoelectric cooler, J. Power Sources 496 (229821) (2021) 1–8, https://doi.org/10.1016/j.jpowsour.2021.229821.
[4] K. Tappura, K. Jaakkola, A thin-film thermoelectric generator for large-area applications, Proceedings 2 (13) (2018 Dec 10) 1–4.
[5] V. Karthikeyan, J.U. Surjadi, J.C.K. Wong, V. Kannan, K.-H. Lam, X. Chen, et al., Wearable and flexible thin film thermoelectric module for multi-scale energy harvesting, J. Power Sources 455 (2020 Apr 15) 1–10.
[6] H. Bottner, J. Nurnus, A. Gavrikov, G. Kuhner, M. Jagle, C. Kunzel, et al., New thermoelectric components using microsystem technologies, J Microelectromech Syst 13 (3) (2004 Jun 07) 414–420.
[7] G.J. Snyder, J.R. Lim, C.K. Huang, J.-P. Fleurial, Thermoelectric microdevice fabricated by a MEMS-like electrochemical process, Nat. Mater. 2 (8) (2003 Aug 01) 528–531.
[8] M. Takashiri, T. Shirakawa, K. Miyazaki, H. Tsukamoto, Fabrication and characterization of bismuth – telluride - based alloy thin film thermoelectric generators by flash evaporation method, SENSOR ACTUAT A-PHYS 138 (2) (2007 Aug 26) 329–334.
[9] J. Kurosaki, A. Yamamoto, S. Tanaka, J. Cannon, K. Miyazaki, H. Tsukamoto, Fabrication and evaluation of a thermoelectric microdevice on a free-standing substrate, J. Electron. Mater. 38 (7) (2009 Jul) 1326–1330.
[10] P. Fan, Z-h Zheng, Y-z Li, Q-y Lin, J-t Luo, G-x Liang, et al., Low-cost flexible thin-film thermoelectric generator on zinc-based thermoelectric materials, Appl. Phys. Lett. 106 (7) (2015 Feb 16) 1–4.
[11] W. Zhu, Y. Deng, M. Gao, Y. Wang, J. Cui, H. Gao, Thin-film solar thermoelectric generator with enhanced power output: integrated optimization design to obtain directional heat flow, Energy 89 (2015 Sep) 106–117.
[12] P. Fan, Z-h Zheng, Z-k Cai, T-b Chen, P-j Liu, X-m Cai, et al., The high performance of a thin-film thermoelectric generator with heat flow running parallel to film surface, Appl. Phys. Lett. 102 (3) (2013 Jan 21) 1–3.
[13] M. Mizoshiri, M. Mikami, K. Ozaki, K. Kobayashi, Thin-film thermoelectric modules for power generation using focused solar light, J. Electron. Mater. 41 (6) (2012 Jun) 1713–1719.
[14] Y. Zhang, C. Lou, X. Li, X. Li, Thin film thermoelectric generators with semimetal thermoelectric legs, AIP Adv. 9 (5) (2019 May) 1–5.
[15] D. Champier, Thermoelectric generators: a review of applications, Energy Convers. Manag. 140 (2017 May 15) 167–181.
[16] K.T. Settaluri, H. Lo, R.J. Ram, Thin thermoelectric generator system for body energy harvesting, J. Electron. Mater. 41 (6) (2011 Jun) 984–988.
[17] Z. Wang, V. Leonov, P. Fiorini, C.V. Hoof, Realization of a wearable miniaturized thermoelectric generator for human body applications, Sensor Actuat A-Phys 156 (1) (2009 Nov) 95–102.
[18] G.J. Snyder, E.S. Toberer, Complex thermoelectric materials, Nat. Mater. 7 (2) (2008 Feb 1) 105–114.
[19] K.T. Wojciechowski, T. Parashchuk, B. Wiendlocha, O. Cherniushok, Z. Dashevsky, Highly efficient n-type PbTe developed by advanced electronic structure engineering, J. Mater. Chem. C (38) (2020 Oct 14) 13270–13285.
[20] Meng Wei, Tian-Bao Chen, Ju-Guang Hu, Shuo Chen, Hong-li Ma, Jing-ting Luo, Guang-Xing Liang, Xiang-Hua Zhang, Ping Fan, Zhuang-Hao Zheng, Effect of organic nano-components on the thermoelectric properties of Sb_2Te_3 nanocrystal thin film, Scr. Mater. 185 (2020) 105–110. Aug.
[21] Zhuang-Hao Zheng, Xiao-Lei Shi, Dong-Wei Ao, Wei-Di Liu, Yue-Xing Chen, Fu Li, Shuo Chen, Xiao-Qing Tian, Xin-Ru Li, Jing-Yi Duan, Hong-Li Ma, Xiang-Hua Zhang, Guang-Xing Liang, Ping Fan, Zhi-Gang Chen, Rational band engineering and structural manipulations inducing high thermoelectric performance in n-type $CoSb_3$ thin films, Nano Energy (2021 March 81) 105683.
[22] Ping Fan, Xiao-lan Huang, Tian-bao Chen, Fu Li, Yue-xing Chen, Bushra Jabar, Shuo Chen, Hong-li Ma, Guang-xing Liang, Jing-ting Luo, Xiang-hua Zhang, Zhuang-hao Zheng, α-Cu2Se thermoelectric thin films prepared by copper sputtering into selenium precursor layers, Chem. Eng. J. 410 (2021 Apr) 128444.
[23] Z. Dashevsky, L. Dudkin, Generator thermoelectric materials, Journal of Thermoelectricity 1 (1993 Jun) 93–100.
[24] J.P. Heremans, B. Wiendlocha, Tetradymites: Bi_2Te_3-related materials, in: C. Uher (Ed.), Materials Aspect of Thermoelectricity, CRS Press, Boca Raton, 2016, pp. 39–93.
[25] O. Ben-Yehuda, R. Shuker, Y. Gelbstein, Z. Dashevsky, M.P. Dariel, Highly textured Bi_2Te_3-based materials for thermoelectric energy conversion, J. Appl. Phys. 101 (11) (2007 Jun 01) 1–6.

[26] L.D. Ivanova, L.I. Petrova, Granatkina YuV, V.S. Zemskov, O.B. Sokolov, Skipidarov SYa, et al., Extruded materials for thermoelectric coolers, Inorg. Mater. 44 (7) (2008 Jul 03) 687–691.
[27] L.D. Ivanova, L.I. Petrova, Grantkina YuV, V.S. Zemskov, O.B. Sokolov, Skipidarov SYa, et al., Extruded thermoelectric materials based on Bi_2Te_3-Bi_2Se_3 solid solutions, Inorg. Mater. 45 (2) (2009 Feb 07) 123–128.
[28] T. Parashchuk, O. Kostyuk, L. Nykyruy, Z. Dashevsky, High thermoelectric performance of p-type $Bi_{0.5}Sb_{1.5}Te_3$ films on a flexible substrate, Mater. Chem. Phys. 253 (2020 Oct 01) 1–8.
[29] Z. Dashevsky, S. Skipidarov, Investigating the performance of bismuth-antimony telluride in novel materials and device design concepts, in: M. Nikitin, S. Skipidarov (Eds.), Novel Thermoelectric Materials and Device Design Concepts, Springer, New York, 2019, pp. 3–21.
[30] L.M. Goncalves, C. Couto, P. Alpuim, A.G. Rolo, F. Völklein, J.H. Correia, Optimization of thermoelectric properties on Bi_2Te_3 thin films deposited by thermal co-evaporation, Thin Solid Films 518 (10) (2010 Mar 01) 2816–2821.
[31] X. Duan, Y. Jiang, Annealing effects on the structural and electrical transport properties of n-type $Bi_2Te_{2.7}Se_{0.3}$ thin films deposited by flash evaporation, Appl. Surf. Sci. 256 (24) (2010 Oct 01) 7365–7370.
[32] L.W. Silva, M. Kaviany, C. Uher, Thermoelectric performance of films in the bismuth-tellurium and antimony-tellurium systems, J. Appl. Phys. 97 (11) (2005 Jun 01) 1–10.
[33] G. Wang, L. Endicott, C. Uher, Structure and transport properties of B_2Te_3 film, in: O. Eibl, K. Nielsch, N. Peranio, F. Völklein (Eds.), Thermoelectric Bi_2Te_3 Nanomaterials, Wiley-VCH Verlag GmbH & Co. KGaA, Weinheim, 2015, pp. 73–98.
[34] E. Symeou, M. Pervolaraki, C.N. Mihailescu, G.I. Athanasopoulos, C. Papageorgiou, T. Kyratsi, et al., Thermoelectric properties of $Bi_{0.5}Sb_{1.5}Te_3$ thin films grown by pulsed laser deposition, Appl. Surf. Sci. 336 (2015 May 01) 138–142.
[35] D. Bourgault, C.G. Garampon, N. Caillault, L. Carbone, J.A. Aymami, Thermoelectric properties of n-type $Bi_2Te_{2.7}Se_{0.3}$ and p-type $Bi_{0.5}Sb_{1.5}Te_3$ thin films deposited by direct current magnetron sputtering, Thin Solid Films 516 (23) (2008 Oct 01) 8579–8583.
[36] H. Obara, S. Higomo, M. Ohta, A. Yamamoto, K. Ueno, T. Iida, Thermoelectric properties of Bi_2Te_3-based thin films with fine grains fabricated by pulsed laser deposition, Jpn. J. Appl. Phys. 48 (8R) (2009 Aug) 1–4.
[37] M. Hemanadhan, Ch Bapanayya, S. C, Simple flash evaporator for making thin films of compounds, J. Vac. Sci. Technol. 28 (2010 Jun) 625.
[38] T. Parashchuk, Z. Dashevsky, K. Wojciechowski, Feasibility of a high stable PbTe:In semiconductor for thermoelectric energy applications, J. Appl. Phys. 125 (24) (2019 June 28) 1–10.
[39] Min Zhang, Wei Liu, Cheng Zhang, Junhao Qiu, Sen Xie, Fuqiang Hua, Yu Cao, Zhi Li, Hongyao Xie, Ctirad Uher, Xinfeng Tang, Thickness-dependent electronic transport induced by in situ transformation of point defects in MBE-grown Bi_2Te_3 thin films, Appl. Phys. Lett. 117 (2020 Oct) 153902.
[40] S.-J. Park, K.-S. Cho, S.-H. Kim, A study on dielectric characteristics of fluorinated polyimide thin film, J. Colloid Interface Sci. 272 (2) (2004 Apr 15) 384–390.
[41] B. Dzundza, L. Nykyruy, T. Parashchuk, E. Ivakin, Y. Yavorsky, L. Chernyak, et al., Transport and thermoelectric performance of *n*-type PbTe films. Physica B Condens, Matter 588 (2020 Jul 01) 1–8.
[42] E.V. Ivakin, I.G. Kisialiou, L.I. Nykyruy, Y.S. Yavorskyy, Optical studies of heat transfer in PbTe:Bi(Sb) thin films, J.Semicond 52 (13) (2018 Dec) 1691–1695.
[43] T. Parashchuk, L. Chernyak, S. Nemov, Z. Dashevsky, Influence of deformation on $Pb_{1-x}InxTe_{1-y}I_y$ and $Pb_{1-x-y}Sn_xIn_yTe$ films. Phys, Status Solidi B (2020 Aug 18) 1–9.
[44] A.V. Butenko, V. Sandomirsky, R. Kahatabi, Z. Dashevsky, V. Kasian, Y. Schlesinger, Pyroelectric effect induced by built-in field of *p*-*n* junction in the quantum paraelectric PbTe: experimental study, Phys. Rev. Lett. (2008 Feb 100) 57603.
[45] B.M. Goltzman, Z.M. Dashevsky, V.I. Kaydanov, N.V. Kolomoetz, Film Thermoelements: Physics and Application, Nauka, Moscow, 1985 (in Russian).
[46] Y. Liu, Y. Zhang, K.H. Lim, M. Ibánez, S. Ortega, M. Li, et al., High thermoelectric performance in crystallographically textured n-type $Bi_2Te_{3-x}Se_x$ produced from asymmetric colloidal nanocrystals, ACS Nano 12 (7) (2018 July 24) 7174–7184.
[47] B. Chen, J. Li, M. Wu, L. Hu, F. Liu, W. Ao, et al., Simultaneous enhancement of the thermoelectric and mechanical performance in one-step sintered *n*-type Bi_2Te_3-based alloys via a facile MgB_2 doping strategy, ACS Appl. Mater. Interfaces 11 (49) (2019 Dec 11) 45746–45754.
[48] H. Cho, S.Y. Back, J.H. Yun, S. Byeon, H. Jin, J.-S. Rhyee, Thermoelectric properties and low-energy carrier filtering by Mo microparticle dispersion in an *n*-type $(CuI)_{0.003}Bi_2(Te,Se)_3$ bulk matrix, ACS Appl. Mater. Interfaces 12 (34) (2020 Aug 26) 38076–38084.
[49] I.T. Witting, T.C. Chasapis, F. Ricci, M. Peters, N.A. Heinz, G. Hautier, et al., The thermoelectric properties of bismuth telluride, Adv. Electron. Mater 5 (6) (2019 Jun) 1–20.
[50] Z.-H. Zheng, et al., Using high thermal stability flexible thin film thermoelectric generator at moderate temperature, Appl. Phys. Lett. (2018 Apr. 112) 163901.
[51] A. Rogalski, Infrared Detectors, Taylor & Francis Group, 2010.
[52] A. Rogalski, Comparison of photon and thermal detector performance. In handbook of Infra-red Detection Technologies, in: M. Henini, M. Razeghi (Eds.), Elsevier, 2002.